Simulation of Concrete Members Affected by Alkali-Silica Reaction with Grizzly

Technical Report · September 2016

DOI: 10.13140/RG.2.2.15061.83688

1 author:

Alain Giorla
Oak Ridge National Laboratory
31 PUBLICATIONS **580** CITATIONS

SEE PROFILE

ORNL/TM-2016/523

Light Water Reactor Sustainability Program

Simulation of Concrete Members Affected by Alkali-Silica Reaction with Grizzly

Alain B Giorla

September 2016

U.S. Department of Energy
Office of Nuclear Energy

ORNL/TM-2016/523

Light Water Reactor Sustainability Program
Fusion and Materials for Nuclear Systems Division

Simulation of Concrete Members Affected by Alkali-Silica Reaction with Grizzly

ORNL/TM-2016/523
M3LW-16OR-0403053

Alain B Giorla

September 2016

Prepared by
OAK RIDGE NATIONAL LABORATORY
P.O. Box 2008
Oak Ridge, Tennessee 37831-6285
managed by
UT-Battelle, LLC
for the
US DEPARTMENT OF ENERGY
Office of Nuclear Energy
under contract DE-AC05-00OR22725

CONTENTS

LIST OF FIGURES

LIST OF TABLES

ACRONYMS

ASR Alkali-Silica Reaction

GSL GNU Scientific Library

LWRS Light Water Reactor Sustainability

MOOSE Multiphysics Object-Oriented Simulation Environment [Gaston et al., 2009]

NPP Nuclear Power Plant

UTK University of Tennessee Knoxville

XFEM Extended Finite Element Method

EXECUTIVE SUMMARY

The analysis of concrete structures affected by degradation mechanisms such as Alkali-Silica Reaction (ASR) requires the development of numerical models based on the underlying physical mechanisms. In turn, such models require validation on a comprehensive set of experiments, which must be conducted at both the material scale and the structural scale, due to the heterogeneous, time-dependent, and non-linear nature of the material.

An ASR structural model was implemented in Grizzly by Huang et al. [2015], based on the work of Saouma and Perotti [2006]. It is combined with a coupled heat-moisture transport model adapted from the work of [Bažant et al., 1982, Xi et al., 1994]. The model was able to reproduce material-level experiments in the literature [Larive, 1997, Ranc et al., 2003, Multon and Toutlemonde, 2006]. In the present work, it is used to simulate structural-level ASR experiments conducted at UTK [Le Pape et al., 2014], in order to validate the use of the model for the analysis of large concrete structures affected by ASR.

The results presented in this report are only preliminary results, since a) the experiments at UTK are not sufficiently advanced to calibrate all material parameters in the model and b) a certain number of components are missing from Grizzly for the simulation of concrete structures subject to chemical or physical degradation. Notably, the following modules are required (in order of priority):

- **Damage.** Concrete is a strongly nonlinear material, with an asymmetric behavior in tension and in compression. A damage model able to capture the complex failure of concrete under load is of utmost importance for any durability or safety analysis.
- **Creep.** The viscoelastic nature of concrete tends to cause stress relaxation. While this may prevent or delay the occurrence of cracking, it may also lead to excessive deformations or the loss of prestress in prestressed tendons.
- **Shrinkage.** Drying of concrete causes shrinkage on the surface, itself leading to possible cracking. Furthermore, shrinkage plays a significant role in the creep mechanism, and a creep model should be coordinated with a drying model.
- **Rebars.** Reinforcements play a significant role in the concrete strength, and an appropriate rebar model, accounting for friction or debonding between the materials, would be required for the analysis of heavily-reinforced concrete structures such as nuclear power plants.

Without these components, simulations of concrete structures with Grizzly remain limited to pure elastic calculations, which are a poor representation of the complex mechanical behavior of the material. Implementing these would make Grizzly a versatile tool for the simulation of concrete durability phenomena in nuclear power plants.

1. INTRODUCTION

In the United States, multiple Nuclear Power Plants (NPPs) have begun the process of a second license renewal, extending their operation from 60 to 80 years. This requires an assessment of the durability of all their components over long periods of time, in particular, the concrete structure itself. Concrete is exposed to multiple aging and degradation mechanisms, and in recent years, several NPP in the world have been diagnosed with ASR: In Japan, Ikata No.1, Shikoku Electric Power [Takatura et al., 2005, Shimizu et al., 2005]; In Canada, Gentilly 2 [Tcherner and Aziz, 2009]; And in the United States, Seabrook [ML121160422, 2012, Saouma and Hariri-Ardebili, 2014].

ASR is a highly complex phenomenon which originates from a chemical reaction between alkali contained in the concrete pore solution and regions of amorphous silica present in the aggregates [Stanton, 1940, Rajabipour et al., 2015]. The product of this reaction is a gel that swells in presence of water, causing an expansion of concrete as well as micro-cracking. ASR is coupled to other processes in concrete such as moisture and temperature transport, and is strongly nonlinear with the structural load. Therefore, numerical models are required to analyze the evolution of the reaction, the expansion and the degradation in a particular structure.

The model from [Saouma and Perotti, 2006] has been implemented in Grizzly by Huang et al. [2015] for its ability to reproduce a number of experiments from the literature, including effects of temperature, relative humidity, and compressive loading. In the present report, the model as implemented in Grizzly is used to simulate a series of ASR experiments conducted at UTK on large-scale reinforced concrete members in free and restrained conditions [Le Pape et al., 2014, Hayes et al., 2016]. The specimens have no shear reinforcements to represent the conditions of some NPP structures in the Uniter States. Such an extensive experimental program can provide a strong basis for the validation and calibration of ASR models for nuclear structures.

The constitutive model from [Saouma and Perotti, 2006] as implemented in Grizzly is first summarized, complemented with a summary of key features associated with ASR. Then, a rigorous method to calibrate material parameters for an ASR constitutive model is described. The model is then used for a preliminary simulation of the large-scale members of the UTK-ASR experimental campaign. Since the experiments only started on July 23rd, 2016, there is not enough experimental data available at this point to compare to the simulation results, nor fully calibrate the numerical model itself.

Therefore, the main outcome of this report is not the numerical results itself, but the experience gained in using Grizzly for the simulation of concrete structures. A set of recommendations for the Grizzly development team is elaborated. Indeed, the current implementation of concrete models in Grizzly is very specific to a single phenomenon and a single model, which in the future will make difficult the coupling between this ASR model and other phenomena such as creep, shrinkage, or irradiation effects. The recommendations provided by the author are aimed at facilitating the integration and coupling of different constitutive models in Grizzly, thus providing the Departement of Energy with a highly versatile toolbox for the simulation of aging concrete structures.

2. ASR CONSTITUTIVE MODEL

Since its discovery in the 1940's, ASR has been the subject of numerous studies, notably because of its relatively high occurence in hydraulic power plants. A number of key features of the underlying chemico-physical processes have been identified, and various models have been proposed to simulate ASR-affected structures. The main aspects of ASR expansion and degradation in structures are first recalled. Then, the model of [Saouma and Perotti, 2006] is presented.

A comprehensive review of the current state of the art of ASR-related research can be found in [Rajabipour et al., 2015], or in [Pan et al., 2012] for ASR models.

2.1 Alkali-Silica Reaction in Structures

ASR is caused by the reaction between alkali ions contained in the concrete pore solution and amorphous silica phases present in the aggregates [Stanton, 1940]. A dissolution-reaction-precipitation mechanism leads to the formation of a gel which swells in presence of water. This swelling occurs in confined spaces (either as a reaction rim around the aggregates for highly reactive aggregates, or as gel pockets located inside the aggregates for the most common slow-reactive aggregates [Ben Haha et al., 2007]), and the pressure exerted by the gel on the solid skeletton leads to micro-cracking. At the macroscopic level, concrete undergoes a free volumetric expansion, as well as a loss of engineering properties (stiffness, strength). From a structural perstective however, the main degradation cause is differential expansion caused by gradients in temperature, humidity, or the geometry of the structure itself [Multon, 2003].

The key features of ASR expansion and degradation are summarized below, completed with indications on how these effects are accounted for in macroscopic models. Some of these effects may be better characterized by mesoscale models [Comby-Peyrot et al., 2009, Dunant and Scrivener, 2010, Alnaggar et al., 2013, Giorla et al., 2015], which are out of the scope of the present report.

- The reaction kinetics is generally taken as a sigmoid function of time, which can be characterized by a latency time (the time it takes before the reaction starts) and a characteristic time (the time it takes for the reaction to complete) [Larive, 1997]. In most models, the parameters for this curve are directly calibrated on standard expansion tests in accelerated conditions. Generally, early models confuse the degree of advancement of the chemical reaction with the expansion itself. While both are related, it is critical to consider them as separate variables in the constitutive model.

- High temperature accelerates the reaction, but it doesn't affect the ultimate expansion [Larive, 1997, Shayan, 1998]. This is generally accounted for in structural models using an Arrhenius-type law, with a different activation energy for the latency time and the characteristic time.

- A low relative humidity reduces the expansion, even preventing it below a certain threshold, as the gel requires water to swell [Olafsson, 1986, Steffens et al., 2003, Poyet et al., 2006]. Models usually account for that effect by multiplying the expansion by a function of the relative humidity [Larive, 1997, Saouma and Perotti, 2006], but some account for it directly in the degree of reaction [Pignatelli et al., 2013].

- The elastic and expansive properties of the gel depend on its chemical composition, including the nature of the alkali ions and its Calcium concentration [Ichikawa and Miura, 2007, Leemann and Lura, 2013, Vayghan et al., 2016]. This effect is generally ignored in numerical models.

- The concrete expansion and micro-cracking depends on the aggregate type and particle size distribution [Multon et al., 2010, Reinhardt and Mielich, 2011, Dunant and Scrivener, 2012b]. Some models use a micro-mechanical framework to derive the concrete expansion from the aggregate

particle size distribution [Multon et al., 2010, Charpin and Ehrlacher, 2012]. However, these models generally assume that the reaction occurs as a rim around the aggregate, which does not represent aggregates commonly found in the field.

- The degradation is delayed by creep when it occurs over long period of time [Giorla et al., 2015]. Only a few recent ASR models account for creep in their formulation [Grimal et al., 2010]. This effect is particularly important to relate short-term experiments to field conditions.
- The expansion and degradation is strongly affected by compressive loads. The expansion in the direction of the load is reduced, and even negated for compressive loads above 10 MPa [Larive, 1997, Berra et al., 2010, Dunant and Scrivener, 2012a]. In multi-axial conditions, the expansion is redistributed along the different orientations, and the total volumetric expansion is non-linearly affected by the load distribution [Multon and Toutlemonde, 2006, Giorla, 2013]. This is a critical aspect of ASR at the structural level, and has been the focus of most recent modelling studies. In earlier models, the total expansion is reduced by a factor depending on the compressive load [Léger et al., 1996]. In the model of Saouma and Perotti [2006], the expansion is reduced in the direction of the load and redistributed in the other directions, depending on the current stress state of an element. In damage-driven models [Capra and Sellier, 2003, Comi and Perego, 2010, Grimal et al., 2010, Pignatelli et al., 2013, Charpin and Ehrlacher, 2014], mechanical loads first affect the mechanical properties of concrete through an anisotropic damage tensor, which is in turn used to derive the concrete expansion.
- Finally, recent studies have shown that alkali leaching has a strong impact in laboratory testing [Chappex et al., 2016, Multon and Sellier, 2016], slowing down the reaction rate after some time, depending on the curing conditions of the sample. This indicates that reaction kinetics parameters identified through laboratory testing, including the maximum expansion, might be lower than their actual values. This effect is not integrated in any structural ASR model to the author's knowledge.

Therefore, a constitutive model for ASR can be expressed using the following relations:

$$\frac{\partial \xi}{\partial t} = f(\xi, T, h, [\text{Na}|\text{K}|\text{Ca}], A) \tag{1}$$

$$\boldsymbol{\sigma} = (\mathbf{1} - \boldsymbol{\omega}(\xi, A, \boldsymbol{\sigma})) : \mathbb{C} : [\boldsymbol{\epsilon} - \boldsymbol{\epsilon}_{\text{ASR}}(\xi, A, \boldsymbol{\sigma})] \tag{2}$$

With ξ the degree of advancement of the chemical reaction (varying between 0 and 1); T the temperature, h the relative humidity, [Na|K|Ca] a factor representing the concentration of alkali and Calcium ions in the pore solution (usually ignored), A a factor accounting for the aggregate reactivity and particle size distribution (usually ignored), $\boldsymbol{\sigma}$ the second-order stress tensor, $\boldsymbol{\epsilon}$ the second-order strain tensor, $\mathbb{C}$ the fourth-order stiffness tensor of the material, $\mathbf{1}$ the second-order identity tensor, $\boldsymbol{\omega}$ the overall second-order damage tensor, and $\boldsymbol{\epsilon}_{\text{ASR}}$ the ASR expansion (also a second-order tensor).

2.2 Saouma and Perotti [2006] ASR constitutive model

The following constitutive model, first developed by Saouma and Perotti [2006] and implemented in Merlin [Reich et al., 1997], was implemented in Grizzly by Huang et al. [2015].

Chemical Reaction

The degree of advancement of the chemical reaction follows a standard sigmoid curve [Larive, 1997]:

$$\frac{\partial \xi}{\partial t} = \frac{(1 - \xi)(\xi + e^{-\tau_L/\tau_C})}{1 + e^{-\tau_L/\tau_C}} \tag{3}$$

With τ_L the latency time and τ_C the characteristic time. These are function of the temperature and the applied stress:

$$\tau_C = \tau_C(T_0)\, e^{U_C\left(\frac{1}{T}-\frac{1}{T_0}\right)} \tag{4}$$

$$\tau_L = \tau_L(T_0)\, f(I_\sigma)\, e^{U_L\left(\frac{1}{T}-\frac{1}{T_0}\right)} \tag{5}$$

$$f(I_\sigma) = \begin{cases} 1 \text{ if } I_\sigma > 0 \\ 1 + \alpha\, \frac{I_\sigma}{3f'_c} \text{ if } I_\sigma < 0 \end{cases} \tag{6}$$

With T_0 the reference temperature, U_C and U_L two activation temperatures, I_σ the first stress invariant, f'_c the concrete compressive strength, and α a coefficient expressing the delay of expansion under compressive stresses ($\alpha > 1$).

While the model represents the expansion under multi-axial load from the literature [Multon and Toutlemonde, 2006, Huang and Spencer, 2016], it has been reported in the literature that compressive stress does not affect the extent of the reaction itself [Larive, 1997]. Furthermore, the model as implemented in Grizzly assumes a constant compressive strength. A reduction of the concrete compressive strength causes negative $\frac{\partial \xi}{\partial t}$ to appear during the nonlinear resolution in Grizzly, which is not physical and causes the nonlinear solver to diverge. Various studies have shown that the compressive strength of ASR-affected concrete diminishes (relatively to that of unreacted concrete at the same age) with the extent of the reaction [Swamy and Al-Asali, 1988, Giaccio et al., 2008, Giannini, 2012].

Damage

The ASR-induced damage in Saouma and Perotti [2006] is isotropic and is a linear function of the chemical advancement:

$$\boldsymbol{\omega} = (1 - \beta_E)\, \xi\, \mathbf{1} \tag{7}$$

With β_E a material parameter describing the relative loss of Young's modulus.

Similarly, the tensile strength f'_t is affected by the reaction as:

$$f'_t = f'_{t,0}\, [1 - (1 - \beta_t)\, \xi] \tag{8}$$

With $f'_{t,0}$ the undamaged tensile strength and β_t another material parameter.

This model assumes that damage occurs homogeneously through the material, even under compressive loading. However, when ASR occurs under compressive loading, cracks tend to develop in the primary direction of the load, and more cracks appear for higher level of load, indicating that damage is oriented with respect to the principal stress direction [Larive, 1997, Multon and Toutlemonde, 2006, Berra et al., 2010, Dunant and Scrivener, 2012a]. More recent models use an anisotropic description of the damage to simulate the effect of applied load on the ASR-induced damage [Grimal et al., 2010, Pignatelli et al., 2013, Charpin and Ehrlacher, 2014].

As discussed above, the model neglects the effect of ASR on the compressive strength.

Expansion

The imposed expansion in Saouma and Perotti [2006] model is anisotropic, and is calculated in three steps:

1. The volumetric ASR strain ϵ_{vol} is calculated from the extent of the reaction ξ and the other state variables.

2. The imposed strain ϵ'_{ASR} is calculated from ϵ_{vol} and the principal stresses σ_i in the coordinates of the principal stresses.

3. The imposed strain in the cartesian coordinates ϵ_{ASR} is obtained by rotating ϵ'_{ASR} by the appropriate three-dimensional angles.

The volumetric ASR strain ϵ_{vol} is given by:

$$\frac{\partial \epsilon_{vol}}{\partial t} = \Gamma_t \, \Gamma_c \, f_h \, \epsilon^{\infty} \, \frac{\partial \xi}{\partial t} \tag{9}$$

Where Γ_t and Γ_c indicate the dissipation of the gel in cracks formed under tension and compression respectively, f_h is a function of the relative humidity, and ϵ^{∞} is the asymptotic expansion.

$$\Gamma_t = \begin{cases} 1 & \text{if } \sigma_I < \gamma_t \, f'_t \\ \Gamma_r + (1 - \Gamma_r) \frac{\gamma_t \, f'_t}{\sigma_I} & \text{if } \sigma_I > \gamma_t \, f'_t \end{cases} \tag{10}$$

$$\Gamma_c = \begin{cases} 1 & \text{if } I_\sigma > 0 \\ 1 - \frac{e^{\beta_c}}{\frac{3 f'_c}{I_\sigma} + (e^{\beta_c} - 1)} & \text{if } I_\sigma < 0 \end{cases} \tag{11}$$

With γ_t the threshold below which no gel dissipation occurs in tension, Γ_r the remaining expansion under high tensile stresses, β_c a parameter controling the rate of dissipation as a function of the compressive stress, f'_t and f'_c the tensile and compressive strength respectively, σ_I the maximum principal stress and I_σ the first stress invariant.

With this model, there is no expansion under very high compressive stresses, but a residual expansion under tensile stress. Several studies on the effect of compressive stress have shown a nonlinear relation between the load and the total volumetric expansion [Larive, 1997, Multon and Toutlemonde, 2006, Berra et al., 2010, Dunant and Scrivener, 2012a]. However, this effect seems to be non-monotonic with the applied stress [Giorla, 2013], thus indicating that another mechanism might be at play. To the author's knowledge, there is no data on ASR under tensile stresses which could confirm the proposed model.

Also, in its original development, Saouma and Perotti [2006] proposed a variant of Eq. (10) when the ASR model is coupled with a smeared crack model. In the current Grizzly implementation, only the formulation described here is available.

The function of relative humidity is taken from the work of Capra and Bournazel [1998] as:

$$f_h = h^m \tag{12}$$

With m a material parameter higher than 1. Bažant and Steffens [2000] chose a linear approximation, while more recent models such as [Comi et al., 2012] incorporate the role of moisture as additional factors in the expression of the characteristic and latency times τ_C and τ_L, thus coupling the influence of temperature and relative humidity on the expansion.

Once the volumetric expansion ϵ_{vol} has been obtained, it is distributed along the direction of the principal stresses depending on their value. Notably, the expansion in one direction is negated if the compressive stress in that direction exceeds a certain threshold σ_u. The expansion in a direction i is multiplied by the appropriate weight:

$$\epsilon'_{ASR,\,ii} = W_i \, \epsilon_{vol} \tag{13}$$

$$\epsilon'_{ASR,\,ij} = 0 \text{ for } i \neq j \tag{14}$$

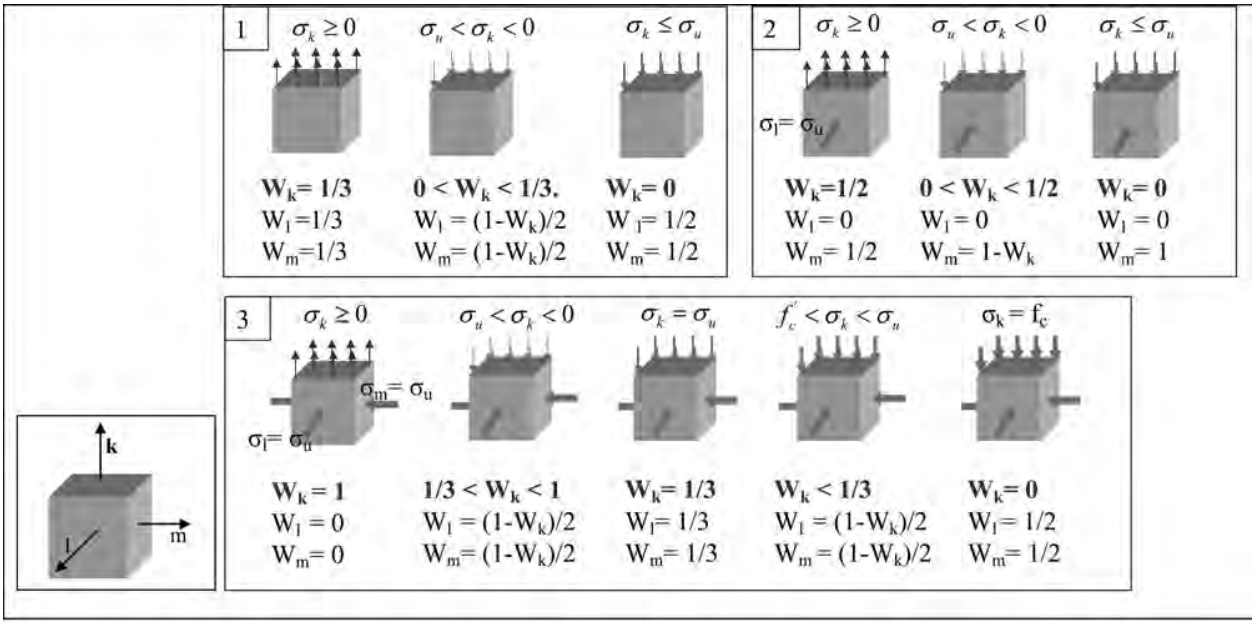

Figure 1. Redistribution of the ASR expansion under multi-axial loads. Figure from [Saouma and Perotti, 2006]

Where W_i depends on the values of the principal stresses relative to the tensile strength, the compressive strength, and the compressive strength threshold. Sixteen cases are indentified depending on the values of the principal stress, as shown in Figure 1. In absence of structural loads, all weights are equal to 1/3 (isotropic expansion).

Once $\boldsymbol{\epsilon}'_{ASR}$ is determined, it is rotated from the principal stress frame into the cartesian coordinates frame:

$$\boldsymbol{\epsilon}_{ASR,\,ij} = \mathbf{M}_{ik}\, \boldsymbol{\epsilon}'_{ASR,\,kh}\, \mathbf{M}_{jh} \tag{15}$$

With $\mathbf{M}$ the 3-dimensional rotation matrix.

For simple cases, the user can force the model to ignore anisotropic effects ($W_i = 1/3\ \forall i$), in which case the rotation is not required.

2.3 Coupled Moisture-Heat Transport Model

In this section, the constitutive equations for the coupled moisture-heat model implemented in Grizzly are briefly summarized. A more comprehensive description of these equations can be found in [Huang et al., 2015]. The ASR model and the moisture-heat transport model are only weakly coupled: In the simulations, the moisture-heat transport system is solved first, and the results are used as input for the mechanical problem.

The set of constitutive equations are adapted from [Bažant et al., 1982, Xi et al., 1994]:

$$\rho_c\, C_c\, \frac{\partial T}{\partial t} = \nabla \cdot (k_c\, \nabla T) + \rho_w\, C_w\, D_w\, \nabla h \cdot \nabla T + C_a\, \mathcal{M}_w\, \frac{\partial h}{\partial t} + Q \tag{16}$$

$$\mathcal{M}_w\, \frac{\partial h}{\partial t} = \nabla \cdot (D_w\, \nabla h) + \nabla \cdot (D_T\, \nabla T) + \frac{\partial W_h}{\partial t} \tag{17}$$

With ρ_c the concrete density, ρ_w the water density (function of temperature), C_c the concrete thermal capacity, C_w the isobaric heat capacity of liquid water (also function of temperature), C_a the adsorption heat (which is generally negligible according to Bažant et al. [1982]), k_c the concrete thermal conductivity, D_w the moisture diffusivity, D_T the moisture diffusivity induced by a temperature gradient, $\mathcal{M}_w$ the moisture capacity of the material, Q the body heat generated (for example, from hydration processes), W_h the mass of free evaporable water released by dehydration of the cement paste (caused by increase of temperature), and the primary unknown being T the temperature and h the relative humidity (ratio between the current vapor pressure and the saturation vapor pressure).

In Grizzly, Huang et al. [2015] implemented various models from the literature for some of the concrete material properties which appear in Eqs (16-17):

- The concrete thermal capacity C_c can either be chosen as a constant, or as a function of temperature. While a few models from the literature are implemented (e.g. [Kodur et al., 2004]), these models rely on fixed material constants (sometimes with a distinction depending on the aggregate type), which may not be valid for all types of concrete.

- The concrete thermal conductivity k_c can also either be chosen as a constant, or using a temperature-dependent model from the literature. Notably, the model of Kim et al. [2003] proposes to compute k_c from the concrete composition (water/cement ratio, aggregate fraction, current relative humidity).

- The moisture capacity $\mathcal{M}$ of the concrete relates to its water adsorption-desorption isotherm . In Grizzly, a model proposed by Xi et al. [1994] based on the Brunauer-Emmett-Teller theory [Brunauer et al., 1938] is implemented, in which the coefficients of the BET curve depend on the water/cement ratio. The model notably distinguishes the contribution from the cement paste and the aggregate porosity. Dependence of the BET curve on temperature [Poyet, 2009] is neglected.

- Several models for the moisture diffusivity are implemented, generally depending on the relative humidity, except Ababneh et al. [2003] (also function of the water-cement ratio) and Bažant et al. [1982] (function of the temperature).

In most cases, the coefficients for these models are fixed by their authors (the values are all reported in [Huang et al., 2015]). However, in certain cases, it might be preferable to give the user the opportunity to use its own function, notably for the concrete themal capacity and conductivity (usually simple functions of the temperature). Also, the moisture capacity model could be extended so that it uses a BET curve provided by the user, instead of the default coefficients.

3. MATERIAL PARAMETERS CALIBRATION

The ASR and heat-moisture models described in the previous section rely on a large number of parameters. In this section, a comprehensive list of these parameters is first established. Then, a methodology to calibrate these parameters from a set of independent experiments is described. It is shown that the ASR experimental campaign launched at UTK [Le Pape et al., 2014, Hayes et al., 2016] provides enough information on the material to calibrate most of these properties.

3.1 List of Material Parameters

The material parameters for the ASR model are listed in Table 1. These parameters do not include usual mechanical properties such as the Young's modulus, Poisson ratio, compressive and tensile strength.

Table 1. List of material parameters for the ASR model

Parameter	Unit	Description
$\tau_L(T_0)$	[day]	Latency time at the reference temperature
$\tau_C(T_0)$	[day]	Characteristic time at the reference temperature
U_L	[K]	Activation temperature for the latency time
U_C	[K]	Activation temperature for the characteristic time
α	[-]	Delay induced by external compressive loading
β_E	[-]	Residual stiffness fraction at the end of the ASR
β_t	[-]	Residual tensile strength fraction at the end of the ASR
ϵ^∞	[m/m]	Volumetric expansion at the end of the ASR
m	[-]	Relative humidity exponent
Γ_r	[-]	Residual expansion for ASR under tensile loading
γ_t	[-]	Threshold in tensile stress above which gel dissipates into cracks
β_c	[-]	Rate at which the gel dissipates into cracks induced by compressive loading
σ_u	[MPa]	Threshold in compressive stress above which expansion is negated

The material parameters for the coupled heat-moisture transport model are listed in Table 2. These parameters do not include concrete composition parameters such as the water/cement ratio, aggregate volume fraction, etc, which may appear in some of the components of the model.

Table 2. List of material parameters for the heat-moisture transport model. (*) indicates a parameter which can be taken as a constant or a function of temperature, humidity, composition, etc.

Parameter	Unit	Description
C_c	[J/kg°C]	Concrete thermal capacity (*)
C_a	[J/kg]	Concrete adsorption heat
k_c	[W/m°C]	Concrete thermal conductivity (*)
D_w	[cm^2/day]	Concrete moisture diffusivity (*)
D_T	[cm^2/day]	Concrete temperature-induced moisture diffusivity
$\mathcal{M}_w$	[kg/kg]	Concrete moisture capacity (*)

3.2 Calibration Methodology

The ASR experimental campaign conducted at UTK is used as a basis to calibrate the different material parameters. When a material parameter cannot be accessed through that campaign, default values are used. The experiments and material testing performed as part of this project are listed in Table 3.

Table 3. List of experiments of the ASR-UTK campaign. (*) indicates experiments performed at Univeristy of Alabama [Giannini, 2016]

Experiment	Concrete	Boundary Conditions	Properties measured
Slab	Non-Reactive	Free	Strains, Temperature
	Reactive	Free	Strains, Temperature
	Reactive	Restrained	Strains, Temperature
Cylinders	Non-Reactive	Free	Mechanical Properties
	Reactive	Free	Mechanical Properties
	Reactive	Restrained	Mechanical Properties
Prism (*)	Free	Non-Reactive	Strain (Shrinkage)
	Reactive	Free	Strain (ASR)
Prism	Non-Reactive	Uniaxial Load	Strain (Basic Creep)
	Reactive	Uniaxial Load	Strain (ASR under compressive load)

All specimen share the same composition. The reactive aggregate (coarse aggregate) is a granite from North Carolina. Lithium nitrate is used as a mitigating agent for the Non-Reactive mix, while sodium hydroxide is added into the mix of the Reactive and Restrained specimens. The Restrained slab is confined in two directions by a rigid still frame [Hayes et al., 2016]. The Restrained cylinders are stored in 6.35mm-thick steel moulds, thus providing a passive restraint similar to the work of Multon and Toutlemonde [2006]. The cylinders are used to measure the concrete Young's modulus, compressive strength and tensile strength (brazilian test) as a function of time.

Numerical Simulations

The calibration is carried out with Grizzly simulations on simplified meshes of the cylinder and prisms tests, as well as the Non-Reactive slab. The simulation of the cylinders are in 2D, assuming rotational symmetry, while the simulations of the prism and the slab are in 3D. The elements are linear, and are either rectangles (2D) or hexagons (3D). The steel reinforcements in the slabs are represented using linear truss elements.

The parameters are obtained using a non-linear least square fitting method using the GSL [Galassi et al., 2009], and implemented in a short dedicated C++ utility program. However, such a capability could be integrated into LWRS tools, for example RAVEN as it already incorporates a control logic framework [Rabiti et al., 2012].

Once the parameters have been calibrated, simulations of the Reactive and Restrained slabs are carried out (see next section).

Calibration Steps

The parameters are calibrated in the following order:

1. ϵ^{∞}, τ_C, τ_L from the Reactive Prism test from University of Alabama (free expansion test).

2. β_E, β_t from the Reactive Cylinder tests.

3. α, β_c and σ_u from the Reactive Prism tests under compressive load.

4. C_c and k_c from the temperature gradient measured in the Non-Reactive slab. The strains in the Non-Reactive slab can also be used to calibrate the concrete thermal expansion.

The following ASR parameters can't be measured from the set of experiments. Typical values from the extensive study of Larive [1997] are taken in the current study.

- Activation temperatures U_C and U_L.
- Parameters related to the dissipation of gel under tensile loading $\Gamma_r,\ \gamma_t$.
- Relative humidity exponent on ASR expansion m.

The following transport-related parameters can't also be measured, notably because the humidity (or water saturation) is not monitored inside the samples.

- Moisture diffusivity D_w and capacity $\mathcal{M}_w$, for which the models of Bažant et al. [1982] and Xi et al. [1994] are used, respectively.
- Temperature-induced moisture diffusivity D_T and concrete adsorption heat C_a, for which default values suggested by Xi et al. [1994] are used.

Preliminary Calibration Results

At the time this report was written, the UTK experiments had just started. Therefore, the only available data to calibrate the model are the prisms tests from University of Alabama [Giannini, 2016]. However, in these experiments, the ASR expansion has not reached its maximum value and is still in the main swelling regime. As such, the asymptotic expansion ϵ_{vol} cannot be characterized yet. It is arbitrarily chosen equal to 0.0054, assuming that the experiments have reached half the maximum expansion.

The following parameters were found:

$$\tau_C(T_0) = 48.7 \text{ [days]} \tag{18}$$

$$\tau_L(T_0) = 188.8 \text{ [days]} \tag{19}$$

The correlation between the experimental expansion and the simulation is shown in Figure 2.

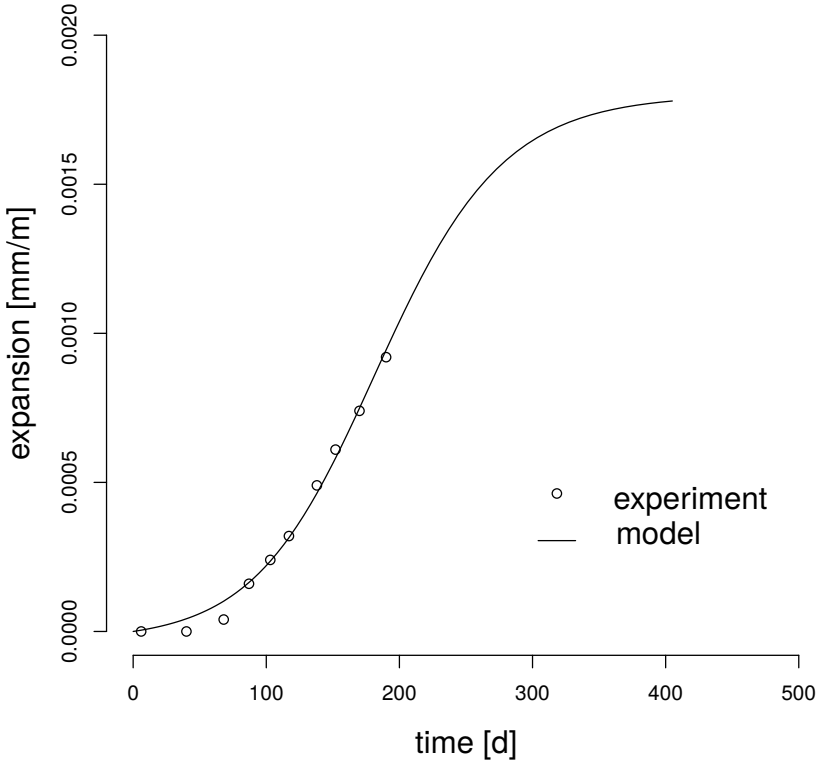

Figure 2. Calibration of the ASR free expansion parameters. Experimental data from [Giannini, 2016]

4. SIMULATION OF FULL-SCALE ASR-AFFECTED CONCRETE MEMBERS

In this section, the simulation of the Reactive (Free) and Reactive (Restrained) slab from the ASR-UTK experimental campaign are described. These are only preliminary simulations, since a) the complementary material testings are not sufficiently advanced at the time this report was written to fully calibrate the model and b) the constitutive model in Grizzly lacks a certain number of key features (from descending order of importance: damage, creep, shrinkage).

First, the material properties of the constitutive model are summarized. Then, the numerical sample and boundary conditions are described, both in terms of mechanics (restraint) and transport (temperature and humidity histories). Finally, the simulation results are presented in terms of temperature, humidity, strain and stress distribution through the sample.

4.1 Material Properties

The material properties for the ASR constitutive model and the moisture-transport model are summarized in Table 4. Values are taken from preliminary testing at University of Alabama [Giannini, 2016] (or fitted from these data, as described in the previous section), or typical value from the literature when unavailable.

Table 4. List of material parameters for the slab simulations

Parameter	Value	Unit	Reference
E	37.8	[GPa]	Measured [Giannini, 2016]
ν	0.3	[-]	Typical value
f'_c	-32.1	[MPa]	Measured [Giannini, 2016]
f'_t	4.3	[MPa]	Measured [Giannini, 2016]
θ	10	[μm/m°C]	Typical value
$\tau_L(T_0)$	188.8	[day]	Calibrated from [Giannini, 2016]
$\tau_C(T_0)$	48.7	[day]	Calibrated from [Giannini, 2016]
U_L	9600	[K]	From [Larive, 1997]
U_C	5400	[K]	From [Larive, 1997]
α	4/3	[-]	From [Saouma and Perotti, 2006]
β_E	0.5	[-]	Assumed
β_t	0.5	[-]	Assumed
ϵ^∞	0.0054	[m/m]	Calibrated from [Giannini, 2016]
m	4	[-]	From [Capra and Bournazel, 1998]
Γ_r	0.8	[-]	From [Saouma et al., 2007]
γ_t	0.5	[-]	Assumed
β_c	0.5	[-]	From [Saouma et al., 2007]
σ_u	-10	[MPa]	From [Saouma et al., 2007]
C_c	0.8	[J/kg°C]	Adapted from [Kodur et al., 2004]
C_a	0.001	[J/kg]	From [Huang et al., 2015]
k_c	1.7	[W/m°C]	Adapted from [Kodur et al., 2004]
D_T	0	[cm^2/day]	Assumed

4.2 Mesh and Boundary Conditions

The samples dimensions are shown in Table 5. The reinforcements are placed in two parallel layers in the Z direction located at 11.34 cm from the surface. The reinforcements form a grid of 11 x 9 rebars equally spaced in the X and Y directions.

Table 5. Dimensions of the concrete slabs (in meters)

Width (X)	Depth (Y)	Thickness (Z)
3.45	2.95	1.02

The sample is meshed with hexagonal linear elements. The ASR and heat-moisture transport simulations use different meshes. The mesh for the heat-moisture transport is non-uniform as it is refined near the surface of the slab to capture gradient effects, and does not include rebars. The mesh for the mechanical simulation is a uniform to which nodes were added at the rebar location (making it non-uniform). A short dedicated C++ software was written to generate meshes compatible with Grizzly, allowing to possibly refine or skew the mesh, or add/remove rebars, using the Exodus II file format [Schoof and Yarberry, 1994].

Meshes for the transport simulation and the ASR simulation are shown in Figure 3 and summarized in Table 6. The steel frame for the Restrained sample is not represented.

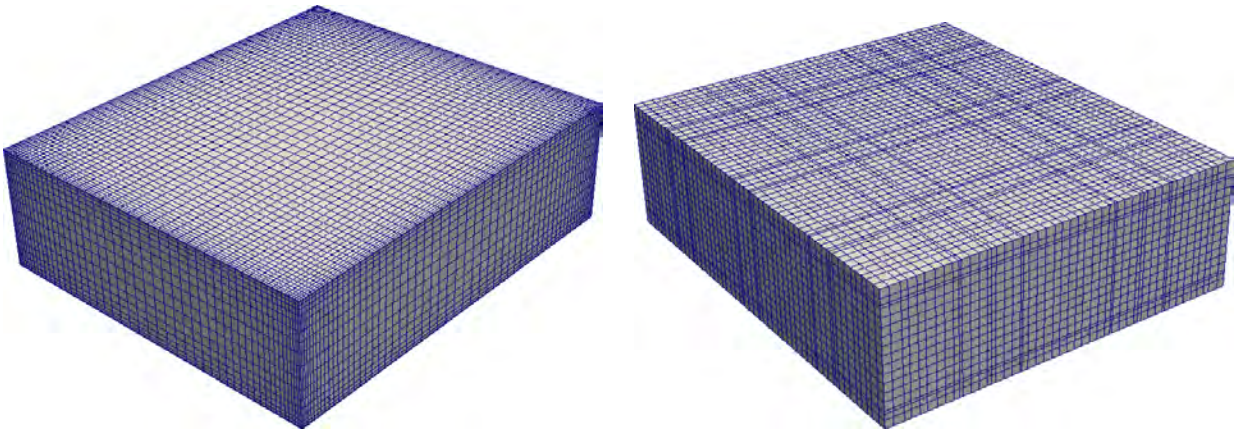

Figure 3. Finite element meshes for the heat-moisture transport simulations (left) and the ASR simulations (right).

Table 6. Number of elements and degrees of freedom for the numerical simulations

Simulation	Elements	dofs
Transport	52,200	114,342
ASR	50,614	159,732

Each sample has six faces: Left/Right in the X direction, Back/Front in the Y direction, and Top/Bottom in the Z direction. The boundary conditions are applied directly on the faces, or on some of the corners of the sample (each corner being defined by three adjacent faces).

Time are expressed in days, with $t = 0$ corresponding to the casting date.

Temperature and Relative Humidity

The temperature and relative humidity histories are shown in Figure 4. The initial rise corresponds to the date at which the climate chamber in which the samples are stored [Hayes et al., 2016] was started, the 12-hours period to reach equilibrium corresponding to the manufacturer's specifications. Daily variations before the installation of the chamber are neglected.

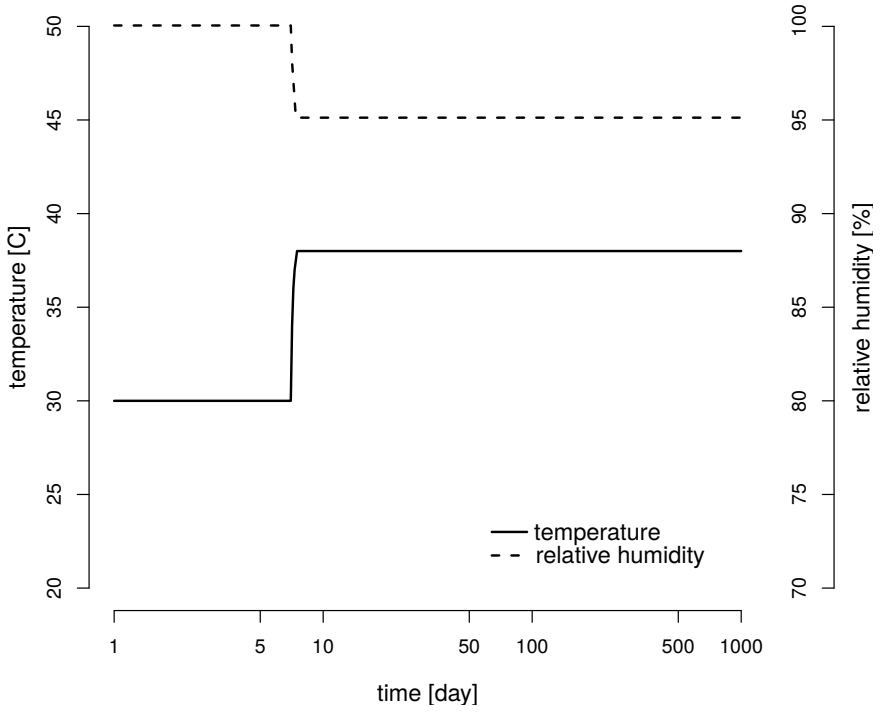

Figure 4. Temperature and relative humidity history imposed at the boundaries of the sample.

The temperature and relative humidity is applied as a Dirichlet boundary conditions on the following faces:

- **Free:** All faces.
- **Restrained:** Top and Bottom only. This neglects the heat transfer between the steel frame and the specimen. The relative humidity condition is correctly represented.

Mechanical

For the ASR simulation, the specimen are subject to the following boundary conditions:

- **Free:** The Bottom-Left-Back corner is fully constrained in all three directions. The Bottom-Left-Front corner can only move in the Y direction, while the Bottom-Right-Back corner can only move in the X direction. The Bottom-Right-Front corner can move in both the X and Y direction. This corresponds to the sample being supported on its four corners, with additional constraints to prevent global rotation or translation of the sample.

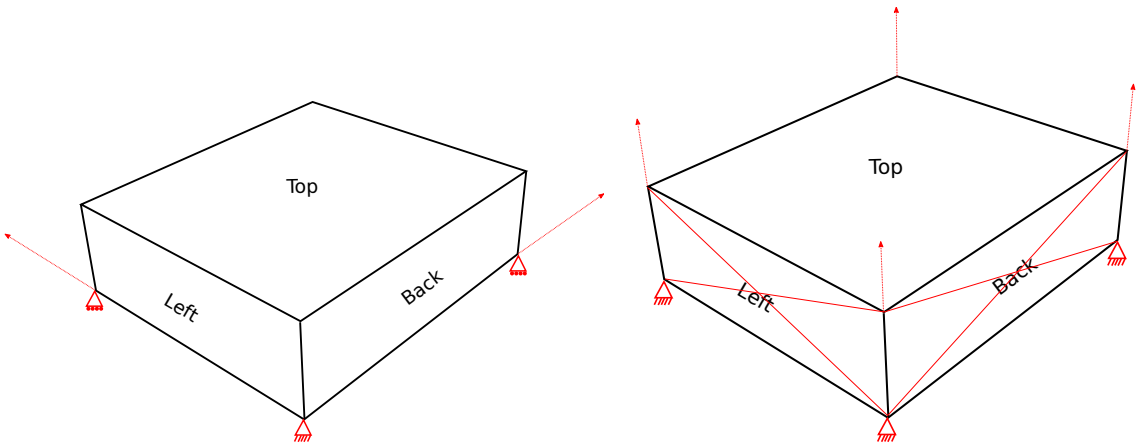

Figure 5. Mechanical boundary conditions for the Free (left) and Restrained (right) specimen. Arrows indicate the direction in which the point of application is allowed to move.

- **Restrained:** The Left, Right, Back and Front faces are assumed to be constrained by the steel frame, and therefore can only move vertically. The four Bottom corners are also fully fixed to prevent global translation of the sample.

These boundary conditions are shown in Figure 5.

Time Steps

Fine time steps are taken during the initial temperature rise, in order to avoid numerical instabilities caused by the thermal shock. Afterwards, the time steps are taken as equally spaced in the logarithimc scale, amounting to a total of 32 time steps. The simulations are run up to 1,095 days (3 years).

4.3 Simulation Outputs

The specimens at UTK are heavily instrumented, with strain transducers, temperature sensors, fiber-optics, acoustic emission sensors, etc. The details of the instrumentation can be found in [Ma et al., 2015].

Grizzly is able to extract the values of the primary variables (temperature, relative humidity, displacements) or auxiliary variables (stress, strain, ASR chemical advancement, etc) at any point in space, allowing to reproduce as best as possible the position of the sensors in the real specimen. However, to limit the amount of data generated (and considering the fact that the model does not account for all the concrete behavior), only a limited number of sensors are simulated at this stage:

- Two sets of four sensors stacked vertically (three inside the sample, one on the Top surface), measuring the strains and stresses in all direction, as well as the temperature and relative humidity. This allows to check the homogeneity of the deformation through the sample, as well as how well surface deformations are correlated with inner deformations.
- One load cell on the Left surface of the Restrained sample, to check the force applied by the ASR on the steel frame.
- Two displacement gauges on the Bottom surface of the sample.

Table 7. Position of the simulated sensors (in meters)

Designation	X	Y	Z
SA1-SA4	1.59	1.34	0.25 / 0.56 / 0.71 / 1.02
SB1-SB4	0.84	0.58	0.25 / 0.56 / 0.71 / 1.02
LC	0	1.50	0.56
DA	0.86 / 2.59	0.71	0
DB	0.71	0.71 / 2.23	0

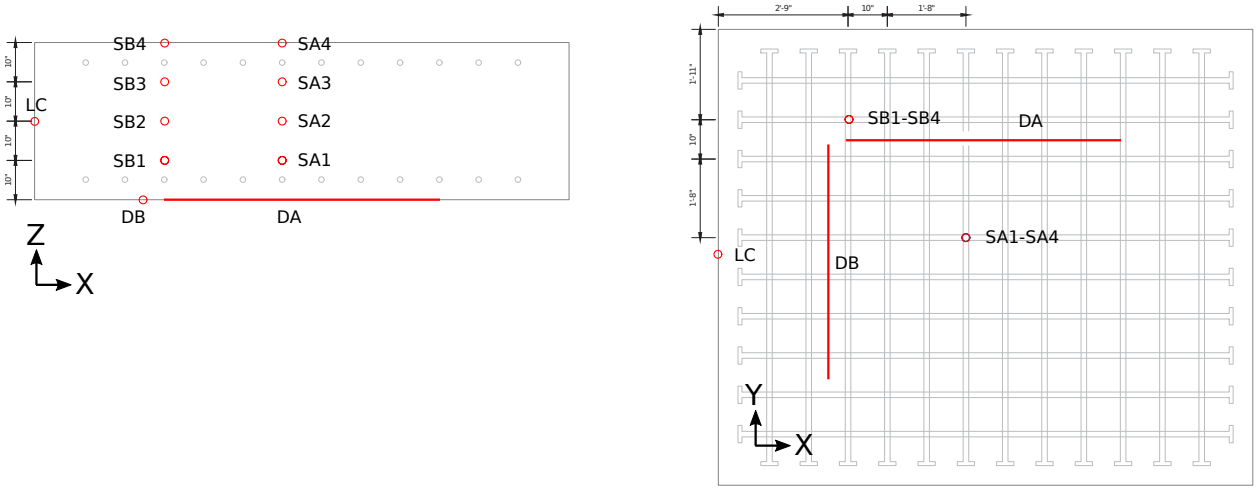

Figure 6. Location of the simulated sensors. Technical drawing adapted from [Ma et al., 2015].

The coordinates of all sensors are listed in Table 7. Their position in the sample are pictured in Figure 6.

5. PRELIMINARY RESULTS

In this section, the results of the simulations are presented.

5.1 Temperature

The temperature as a function of time for the sensors SA1-SA4 and SB1-SB4 are shown in Figure 7. There is an approximately 10 days delay before the temperature inside the specimen stabilizes.

In both specimen, the gradient is the highest in the Z direction. For the Restrained specimen, there is no horizontal gradient, which is consistent with the boundary conditions imposed.

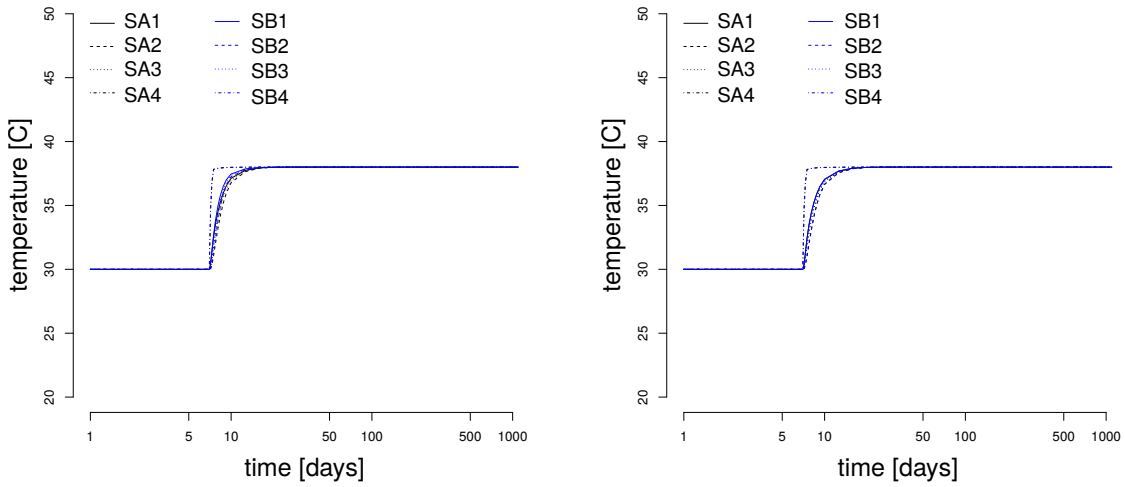

Figure 7. Temperature of the SA1-SA4 (black) and SB1-SB4 (blue) sensors for the Free (left) and Restrained (right) specimen.

The temperature profiles 12 hours after the initial heatings are shown for the Free and Restrained samples in Figure 8.

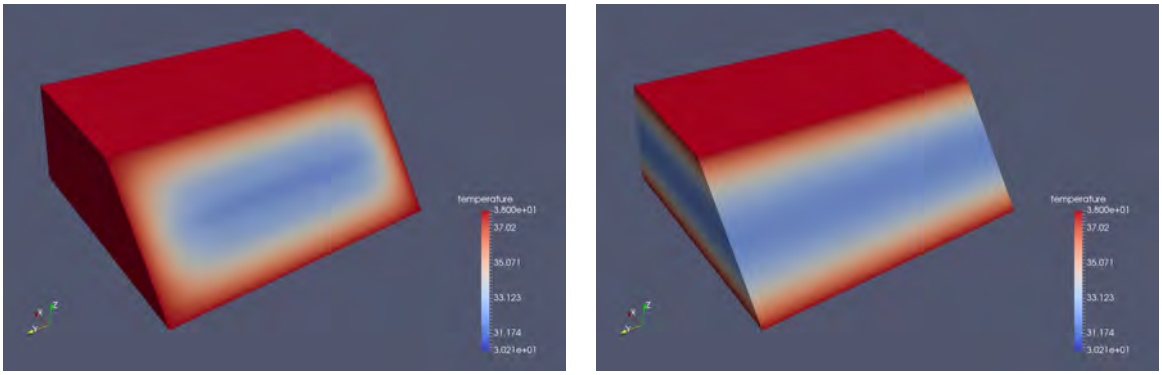

Figure 8. Temperature profile 12 hours after heating for the Free (left) and Restrained (right) specimen.

5.2 Relative Humidity

The relative humidity as a function of time for the sensors SA1-SA4 and SB1-SB4 are shown in Figure 9. The simulations predicts that only a thin layer at the surface of concrete dries, and that the core of the sample remains saturated. Therefore, it is expected that the reaction occurs homogeneously through both samples.

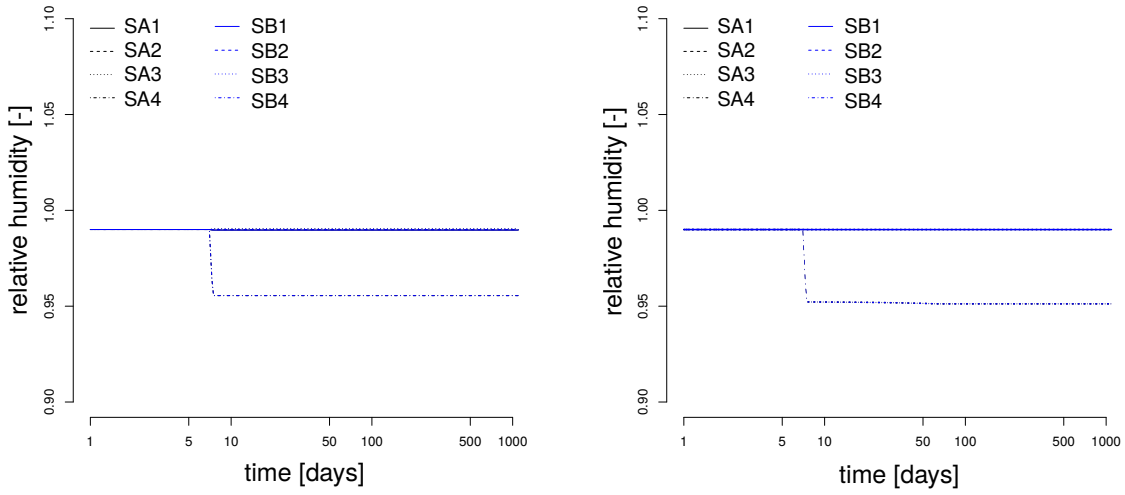

Figure 9. Relative humidity of the SA1-SA4 (black) and SB1-SB4 (blue) sensors for the Free (left) and Restrained (right) specimen.

5.3 Strains

The strains in X, Y and Z directions are shown as a function of time for the sensors SA1-SA4 and SB1-SB4 in Figure 10.

- In the Free specimen, the rebars cause a passive restraint in the horizontal plane. This causes the expansion in the X and Y direction to be lower than in the Z direction.
  - In the center of the specimen (sensors SA1-SA4), the strains are homogeneous through a vertical section. At that point, the surface strains provide therefore a good estimation of the inner deformation.
  - For the sensors SB1-SB4, there is a small strain gradient in the vertical direction. Notably, the surface strain in the X and Y directions are lower than in the bulk. This effect is more prominent in the Y direction than in the X direction. This might be due to the difference in reinforcement ratio in the two directions.
- In the restrained specimen, the expansion in the X and Y directions are both null. The vertical expansion is higher than for the Free specimen, but the total volumetric expansion is lower and develops later. There is no apparent gradient in the vertical expansion at either of the sensors.

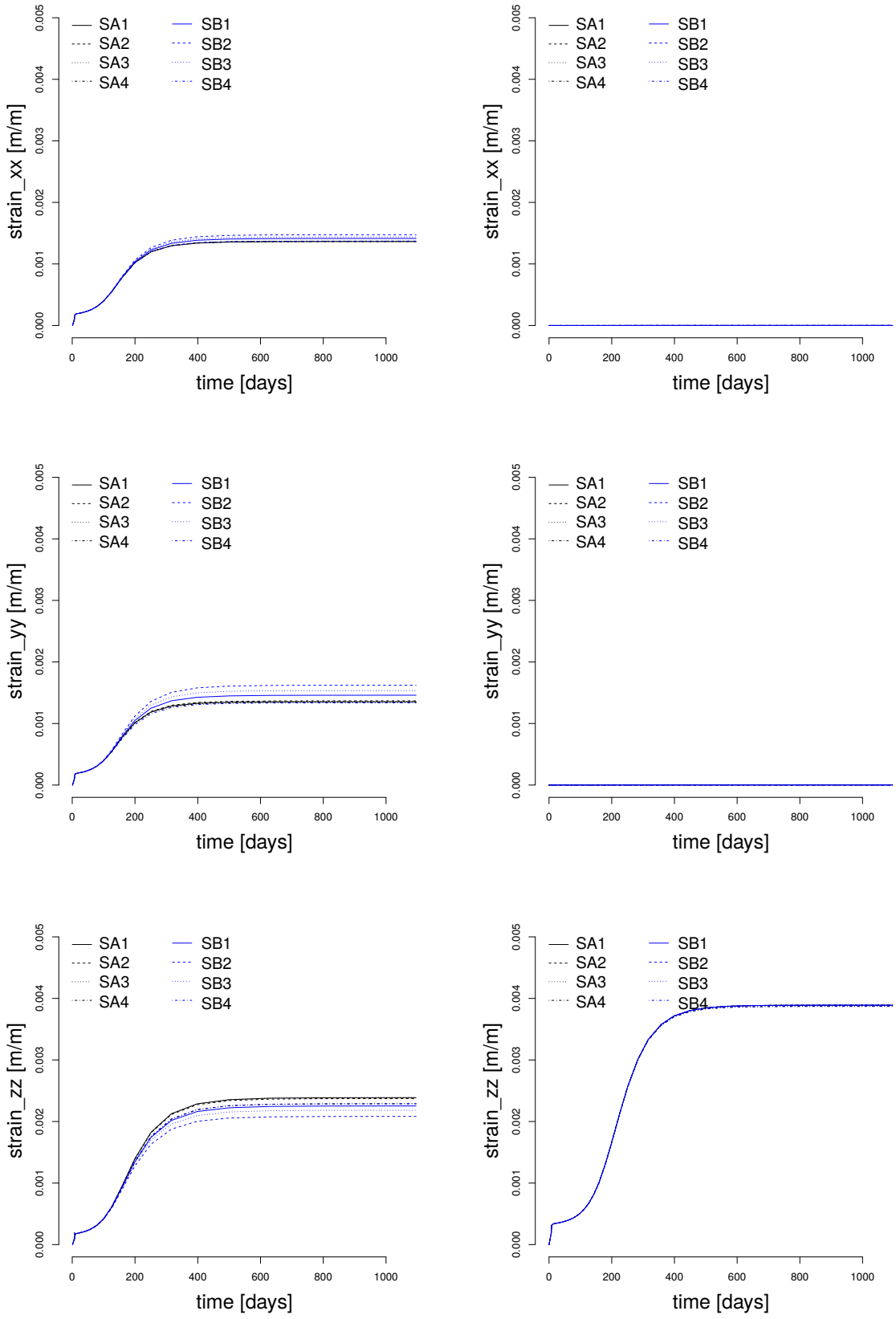

Figure 10. Strain in the X direction (top), Y direction (middle) and Z direction (bottom) of the SA1-SA4 (black) and SB1-SB4 (blue) sensors for the Free left) and Restrained (right) specimen.

The vertical strain and stress in the Free samples after 3 years of reaction are shown in Figure 11. The high stress on the surface of the specimen is due to gradients in relative humidity, as the expansion is lower at the surface than in the core. This indicates that surface cracks might be expected on the surface of the specimen, but this might also be an artifact of the coarse resolution of the mesh.

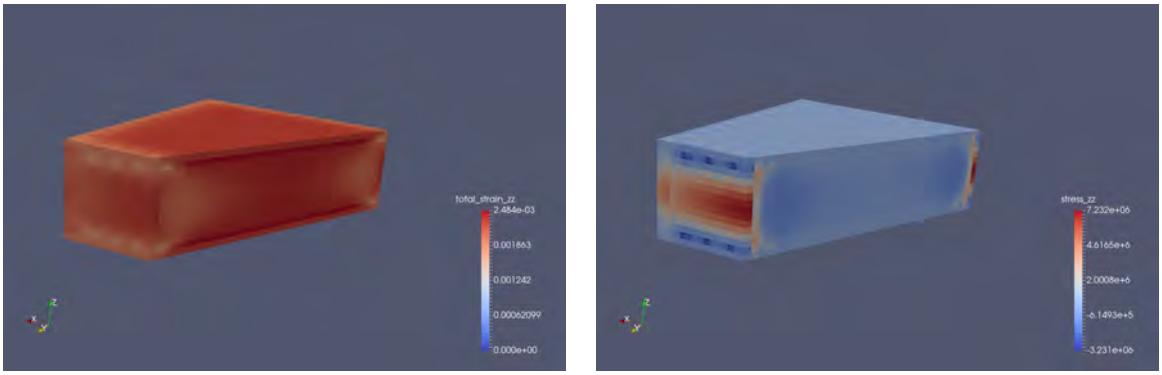

Figure 11. Vertical strain (left) and stress (right) profiles in the Free specimen after 3 years of reaction.

5.4 Lateral Pressure

The lateral pressure imposed by the confined specimen on its steel cage is shown in Figure 12. The pressure quickly raises and is then progressively reduced as ASR goes onward.

This initial rise is due to the fact that the steel frame is simulated by imposing a null displacement on the surface of the specimen. This initial stress is first due to the thermal expansion of the specimen itself, the thermal expansion of the frame being neglected. The following reduction in lateral stress is caused by the loss of elastic modulus caused by ASR.

The boundary conditions are therefore not well captured by the model, and a more advanced model is required (possibly including contact between the specimen and the steel frame).

5.5 Surface Displacements

For the Restrained specimen, there were no deformations measured on the bottom surface due to the boundary conditions. For the Free specimen, the strains measured from the displacements on the bottom surface show a good correlation with the strain measured in the center of the specimen (sensor SA2), but are lower than the strains measured at the sensor SB2 (see Figure 13).

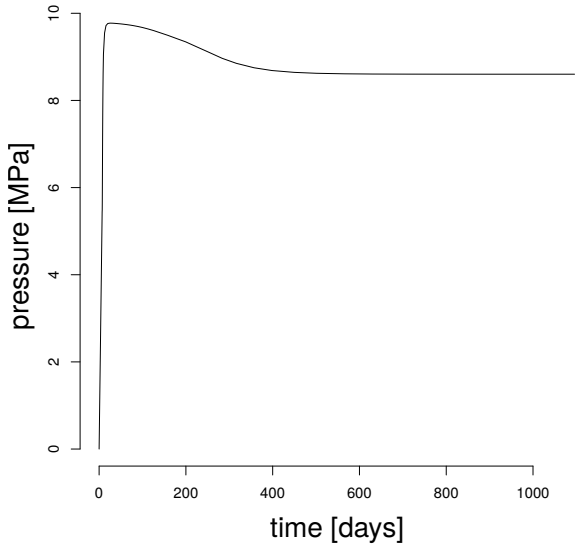

Figure 12. Lateral pressure at the surface of the Restrained specimen.

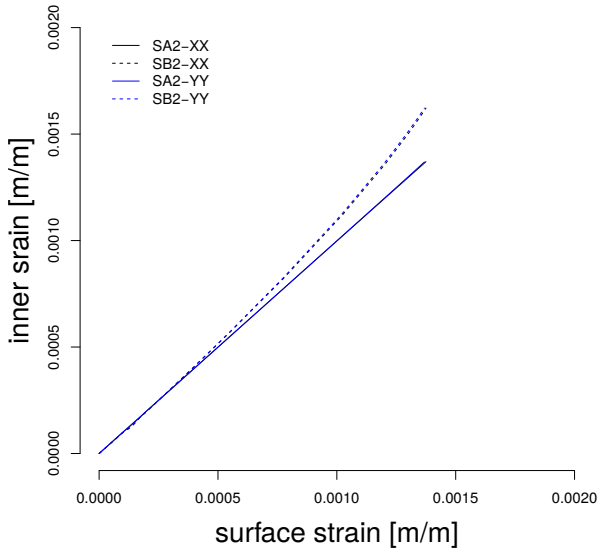

Figure 13. Strains in the middle of the specimen as a function of the strain measured at the surface.

5.6 Discussion

While this report only covers preliminary simulations of the ASR-UTK campaign, it provides a certain number of insights on the possible outcome of the experiments. The main points are:

- Temperature and relative humidity are homogeneous accross the specimen.
- Surface strains are representative of the middle of the specimen only. A vertical strain gradient exists in the specimen up to a depth of 50-75 cm from the lateral surfaces.
- The reinforcements alone provide enough restraint to orient the deformation in the vertical direction.
- The deformation in the X direction seems more homogeneous than the deformation in the Y direction, presumably due to the difference in geometry and reinforcements.

However, a certain number of components are missing from the model, which then requires refinement before providing conclusions.

- The boundary conditions in the Restrained specimen overestimate the actual boundary conditions in the experiment. The steel frame must be either modelled explicitely, or accounted for using a conditional boundary condition.
- The concrete model lacks a nonlinear (damage) component. The ASR model is not enough to capture the complexity of the concrete behavior, including its strong nonlinearity and asymmetry in tension/compression.
- Similarly, the model doesn't account for creep, which has a certain influence of the damage development induced by ASR. Shrinkage is also a missing component. While shrinkage is not a critical phenomenon in this scenario, it might be a major aspect in nuclear power plants, and therefore, should be included in Grizzly as well.

Recommendations on the integration of these two components (damage model, creep/shrinkage model) in Grizzly are presented in the next section.

6. RECOMMENDATIONS FOR THE DEVELOPMENT OF CONCRETE CONSTITUTIVE MODELS IN GRIZZLY

In this section, a series of recommendations are established for the Grizzly development team.

The aim of these recommendations is to facilitate the future integration of constitutive models for concrete, whether they are related to damage, creep, alkali-silica reaction, shrinkage, rebars, corrosion, irradiation, etc.

Concrete is a multi-phase material, and depending on its environment, various chemical, mechanical or physical phenomena might be occuring. It means that the list of models necessary to analyze one concrete structure can vary on a case by case basis, and it is the engineer's decision to account or neglect a certain phenomena in the simulation. Therefore, Grizzly requires a platform through which the list of components can be easily chosen by the user.

If constitutive models are implemented separately, without some form of wraping architecture, then the combinations of several of these models requires additional implementation effort. With the proper software architecture, once each model is implemented separately, arbitrary combinations can be easily achieved. The present section discusses how such a wraping architecture can be implemented in Grizzly.

These recommendations focus on the mechanical behavior of concrete. Similar ideas can be formulated for the heat-moisture transport framework.

6.1 Multi-Mechanics Constitutive Model

To showcase the limitations of the current Grizzly implementation, we use a creep-damage model coupled with ASR, drying shrinkage and thermal expansion. In the following, $\mathbb{C}$ is the fourth-order stiffness tensor of the material, $\boldsymbol{\sigma}$ the second-order stress tensor and $\boldsymbol{\epsilon}$ the second-order strain tensor.

Damage Model

There are a lot of concrete non-nonlinear models in the literature. For sake of simplicity, we use here the model of [Mazars, 1986]:

$$\boldsymbol{\sigma} = (1 - (h_t\, d_t + (1 - h_t)\, d_c))\, \mathbb{C} : \boldsymbol{\epsilon} \tag{20}$$

With d_t and d_c the damage in tension and compression respectively, and h_t a coefficient depending on the current strain orientation. These three scalars are function of the strain.

Creep Model

As for damage, there is a wide range of creep models in the literature. The numerical implementation of these models rely on the use of Kelvin-Voigt or Maxwell chains, which are then integrated using some form of finite differences [Zienkiewicz et al., 1968]. For example, a generalized Maxwell model can be summarized as:

$$\boldsymbol{\sigma} = \left[\mathbb{C} + \sum_i \mathbb{C}_i^{eq}\right] : \left[\boldsymbol{\epsilon} - \sum_i \boldsymbol{\epsilon}_i^{eq}\right] \tag{21}$$

With $\mathbb{C}_i^{eq}$ depending on the stiffness and viscosity of the i^{th} Maxwell module in the chain, and $\boldsymbol{\epsilon}_i^{eq}$ depending on the strain and strain rate in the i^{th} dashpot in the chain. Due to the finite difference implementation, both the apparent stiffness and the apparent creep strain depend on the time step. In some non-linear creep models, the apparent stiffness may also depend on the stress.

ASR Model

As described in section 2, an ASR model can be summarized as:

$$\boldsymbol{\sigma} = (\mathbf{1} - \boldsymbol{\omega}_{ASR}(\xi)) : \mathbb{C} : [\boldsymbol{\epsilon} - \boldsymbol{\epsilon}_{ASR}(\xi)] \tag{22}$$

With ξ the advancement of the chemical reaction, $\boldsymbol{\omega}_{ASR}$ the damage (a second-order tensor) and $\boldsymbol{\epsilon}_{ASR}$ the imposed ASR deformation. Both the ASR damage and expansion also depend on the current level of stress.

Shrinkage Model

A simple shrinkage model might be considered as:

$$\boldsymbol{\sigma} = (1 - d_w(w))\ \mathbb{C} : [\boldsymbol{\epsilon} - \boldsymbol{\epsilon}_{sh}(w)] \tag{23}$$

With w the weight loss, d_w the micromechanical damage caused by the strain mismatch between aggregates and cement paste, and $\boldsymbol{\epsilon}_{sh}$ the shrinkage itself. Models can alternatively be written as a function of the water saturation, the relative humidity or the capillary pore pressure, but the constitutive equation for the mechanical system is the same in all cases.

Thermal Expansion

Assuming that the temperature is low enough to limit dehydration of the cement paste hydrates, the thermal expansion symply reads:

$$\boldsymbol{\sigma} = \mathbb{C} : [\boldsymbol{\epsilon} - \boldsymbol{\epsilon}_T(T)] \tag{24}$$

With $\boldsymbol{\epsilon}_T$ the thermal expansion, a function of the temperature (and in some models also function of the relative humidity).

Combined Model

Combining all the models above gives the following relation:

$$\begin{aligned} \boldsymbol{\sigma} \quad = \quad & [(1 - (h_t\, d_t + (1 - h_t)\, d_c))\, (\mathbf{1} - \boldsymbol{\omega}_{ASR}(\xi))\, (1 - d_w(w))] : \left[\mathbb{C} + \sum_i \mathbb{C}_i^{eq}\right] : \\ & \left[\boldsymbol{\epsilon} - \boldsymbol{\epsilon}_{ASR}(\xi) - \boldsymbol{\epsilon}_{sh}(w) - \boldsymbol{\epsilon}_T(T) - \sum_i \boldsymbol{\epsilon}_i^{eq}\right] \end{aligned} \tag{25}$$

In a more generic form, this can be written as:

$$\boldsymbol{\sigma} = \left[\coprod_p f_p(\mathbb{C}, \alpha_p)\right] : \left[\boldsymbol{\epsilon} - \sum_p \boldsymbol{\epsilon}_p(\alpha_p)\right] \tag{26}$$

With $\coprod$ the function composition operator, and for each phenomenon p: α_p a set of internal variables describing the evolution of the phenomenon (damage, chemical reaction, etc), f_p a function representing the evolution of the stiffness with the α_p, and $\boldsymbol{\epsilon}_p$ the stress-free deformation induced by the phenomenon. Notably, most models affect both the apparent stiffness of the material and the stress-free deformation.

6.2 Limitation of the Current Grizzly Implementation

The current Grizzly implementation uses the `SolidModel` class as the base class to represent concrete, as implemented in the `SolidMechanics` MOOSE module [Hales et al., 2012]. This class accomodates for one `ConstitutiveModel` object that describes the evolution of the stiffness as a function of some internal variables. Using the formalism described above, the main role of a `ConstitutiveModel` is to apply the function $f_p(\mathbb{C}, \alpha_p)$. In addition to the `SolidModel`, Grizzly can accomodate a list of `VolumetricModel` which all apply a form of imposed expansion. With the formalism described above, these `VolumetricModel` apply the stress-free deformations $\boldsymbol{\epsilon}_p(\alpha_p)$. Grizzly can account for an arbitrary number of these volumetric models, which are then summed accordingly. This limits the adaptability of Grizzly in two different ways:

- The composition of multiple models can only be achieved by actually implementing the composed model. This is not a sustainable approach, especially considering the large number of models that were developped in the literature for each separate phenomenon. Not only this is a concern in terms of implementation time due to duplicate work, but also in term of software maintenance. The best approach is to implement each model independently, and implement the generic architecture to make arbitrary compositions, thus allowing the user to use whichever model fits its needs.
- Each phenomenon requires the implementation and use of two separate classes. This is confusing as, from a physical point of view, these are two facets of the same coin. It also requires additional implementation effort compared to an architecture with a unique class for each phenomenon, and it might lead to error during usage, as the user might inadvertently use only one of the two components.

Therefore, the author strongly advocates for a change in the way constitutive models for concrete are implemented. This change should be performed before any more constitutive models are implemented in Grizzly, and is critical for the usability of Grizzly to analyze concrete structures. It can be summarized as:

- Allow the use of multiple `ConstitutiveModel` objects
- Merge the `VolumetricModel` and `ConstitutiveModel` into the same object

In the future, the concrete modeling would be transfered from the `SolidMechanics` module to the `TensorMechanics` module.

6.3 Proposed Framework

The proposed change would require the implementation of two classes in Grizzly:

- `ConcreteSolidModel`: This class is in charge of managing the different constitutive models, similarly to the `SolidModel` class. It also contains its basic mechanical properties so that these can be accessed easily by other submodels.
- `ConcreteConstitutiveModel`: This is an abstract class which serves as a blank framework for the different phenonmenon-based models. As a representation of a single physical phenomenon, it is responsible for storing and updating the α_p, and providing both f_p and $\boldsymbol{\epsilon}_p$.

Tentative skeletons for these two classes are described below:

```
class ConcreteConstitutiveModel
{
  MaterialProperty<T> _internal_variable;
  // repeat for as many variables required by the model

  virtual bool linearUpdate( SymmTensor & current_stress, SymmTensor & current_strain );
  virtual bool nonlinearUpdate( SymmTensor & current_stress, SymmTensor & current_strain );
  virtual bool updateElasticityTensor( SymmElasticityTensor & elasticityTensor );
  virtual bool modifyStrain( SymmTensor & strain_increment );
};

class ConcreteSolidModel
{
  MaterialProperty<Real> & _youngs_modulus;
  MaterialProperty<Real> & _poisson_ratio;
  MaterialProperty<Real> & _tensile_strength;
  MaterialProperty<Real> & _compressive_strength;

  std::vector<ConcreteConstitutiveModel *> & _constitutive_models;

  virtual bool linearUpdate( SymmTensor & current_stress, SymmTensor & current_strain )
  {
    bool update = false;
    for(size_t i = 0 ; i < _constitutive_models.size() ; i++)
      update |= _constitutive_models[i]->linearUpdate( current_stress, current_strain ) ;
    return update ;
  }

  // the following methods use a similar implementation as linearUpdate
  virtual bool nonlinearUpdate( SymmTensor & current_stress, SymmTensor & current_strain );
  virtual bool updateElasticityTensor( SymmElasticityTensor & elasticityTensor );
  virtual bool modifyStrain( SymmTensor & strain_increment );
};
```

Each constitutive model would have four inherited methods, which play a different role in the simulation:

- `linearUpdate` updates the value of the internal variables α_p at the start of each time step. For example, this would be updating the creep strain (finite difference step) or the shrinkage/thermal expansion (as a priori, the mechanical problem is only chained to the heat-moisture transport problem, and not coupled).
- `nonlinearUpdate` updates the value of the internal variables α_p during the non-linear iterations. This is mostly related to the progress of damage (or plasticity) under load.
- `updateElasticityTensor` provides the function f_p as a function of the α_p.
- `modifyStrain` provides ϵ_p as a function of the α_p.

Furthermore, `ConcreteSolidModel` defines the basic mechanical properties of concrete, so that they can be accessed and shared by the different `ConcreteConstitutiveModel` objects. This notably ensures that they are only defined once in the initiation file, thus limiting the risk of errors from the user.

At each time step, these methods would be used in the following workflow:

1. At the start of each time step, update all α_p with `linearUpdate`.
2. Calculate the apparent stiffness using the f_p and the stress-free deformations $\boldsymbol{\epsilon}_p$ as a function of the new α_p.
3. Solve the finite element system. This gives a new $\boldsymbol{\sigma}$ and $\boldsymbol{\epsilon}$.
4. If there are non-linear models, update their α_p with `nonlinearUpdate`.
5. Repeat steps 2 to 4 until all non-linear models have reached convergence.
6. Go to the next time step.

This procedure is depicted in Figure 14. It is similar to what was implemented as part of the XFEM module by [Dolbow et al., 2015]. Exact implementation may depend on the exact MOOSE architecture.

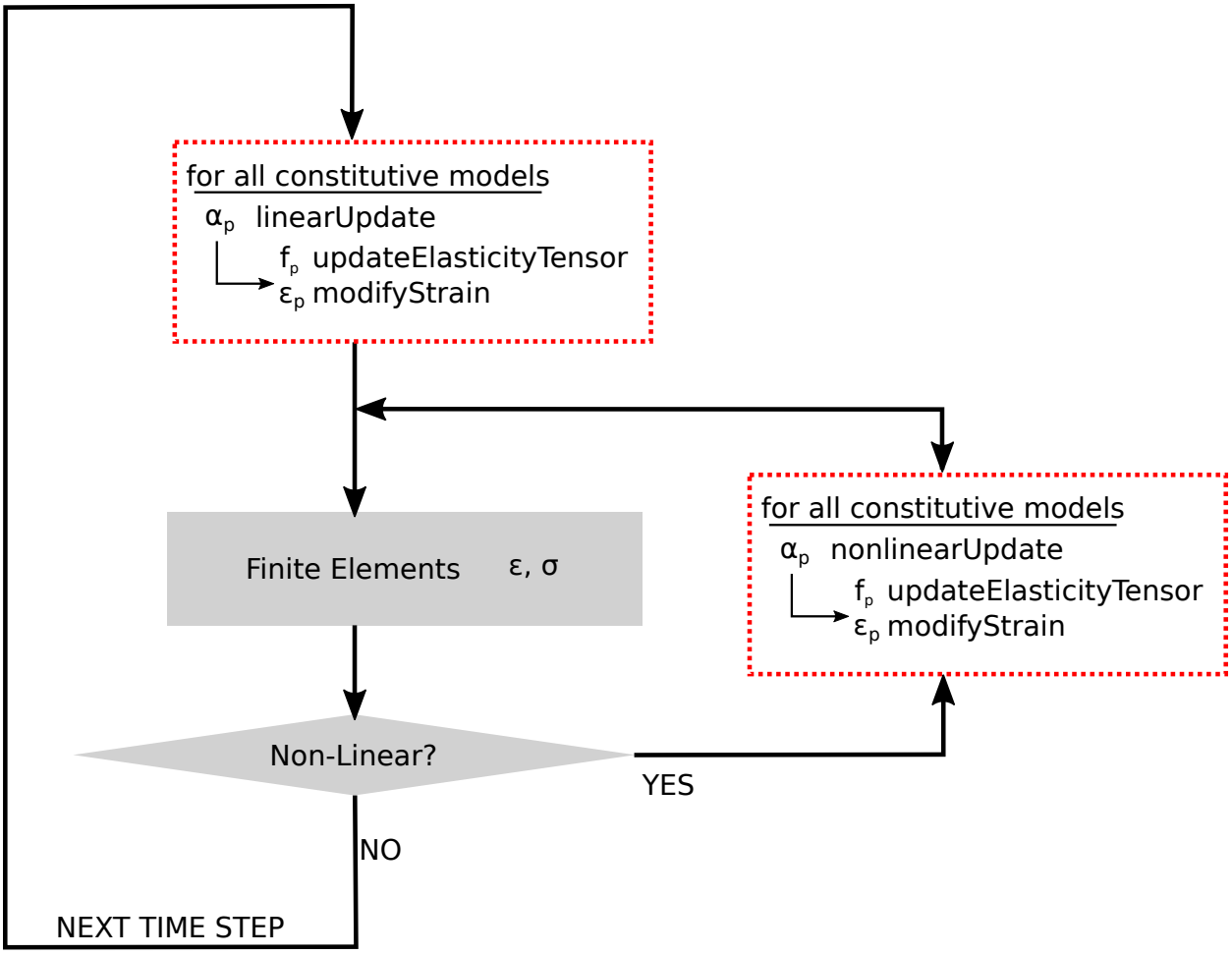

Figure 14. Example of finite element workflow for concrete

7. CONCLUSION

The ASR model of [Saouma and Perotti, 2006], as implemented in Grizzly [Huang et al., 2015], was used to simulate large-scale concrete members of the ASR-UTK experimental campaign [Hayes et al., 2016]. These simulations highlighted the fact that temperature and relative humidity should remain homogeneous through the specimen, and that surface strains would only be representative of the deformations in the middle of the specimen, as vertical gradients exist close to the lateral surfaces.

However, these are preliminary results only. First, the experiments at UTK have just started, and the companion material characterization experiments are not sufficiently advanced to fully calibrate the model. Second, a certain number of components are missing in the simulation. From descending order of priority, the model lacks:

- A nonlinear, multiaxial, constitutive damage law for concrete, able to reproduce the difference in behavior in tension and compression.
- A creep model in order to account for stress relaxation processes over time, possibly limiting the extent of cracking in the material. Such a model should be completed with a drying shrinkage model.
- A model for the rebars and their cohesion with concrete.

To simulate this specific set of experiments, a better representation of the confinment imposed by the steel frame is also required, either by meshing it explicitely, or by applying the mechanical boundary conditions after the initial heating.

However, the author found that the current implementation of constitutive models in Grizzly does not allow an easy coupling between the different components of the concrete behavior (damage, creep, shrinkage, chemically- or physically-induced volumetric expansion). The main limitations are:

- Only one model can modify the apparent stiffness of the material at a time, which notably means that the coupling between mechanical damage, creep and chemically- or physically-induced damage cannot be achieved easily.
- For each phenomenon, a set of two classes are required, one to affect the apparent stiffness and another one to modify the imposed expansion, which should be combined into a single class as these are two facets of the same phenomenon.

It is the author belief that these limitations should be adressed by the Grizzly development team *before* any further work on concrete constitutive models is carried out.

Once these changes have been implemented, the simulations presented in this report can be updated, notably to include the initial results of the ASR-UTK experimental campaign.

7. REFERENCES

A. Ababneh, F. Benboudjema, and Y. Xi. Chloride penetration in nonsaturated concrete. *Journal of Materials in Civil Engineering*, 15(2):183–191, 2003.

M. Alnaggar, G. Cusatis, and G. Di Luzio. Lattice discrete particle modeling (ldpm) of alkali silica reaction (asr) deterioration of concrete structures. *Cement and Concrete Composites*, 41:45–59, 2013.

Z. Bažant and A. Steffens. Mathematical model for kinetics of alkali–silica reaction in concrete. *Cement and Concrete Research*, 30(3):419–428, 2000.

Z. Bažant, J. Chern, and W. Thonguthai. Finite element program for moisture and heat transfer in heated concrete. *Nuclear Engineering and Design*, 68(1):61–70, 1982.

M. Ben Haha, E. Gallucci, A. Guidoum, and K. Scrivener. Relation of expansion due to alkali silica reaction to the degree of reaction measured by sem image analysis. *Cement and Concrete Research*, 37(8): 1206–1214, 2007.

M. Berra, G. Faggiani, T. Mangialardi, and A. Paolini. Influence of stress restraint on the expansive behaviour of concrete affected by alkali-silica reaction. *Cement and Concrete Research*, 40(9):1403–1409, 2010.

S. Brunauer, P. Emmett, and E. Teller. Adsorption of gases in multimolecular layers. *Journal of the American chemical society*, 60(2):309–319, 1938.

B. Capra and J.-P. Bournazel. Modeling of induced mechanical effects of alkali-aggregate reactions. *Cement and Concrete Research*, 28(2):251–260, 1998.

B. Capra and A. Sellier. Orthotropic modelling of alkali-aggregate reaction in concrete structures: numerical simulations. *Mechanics of materials*, 35(8):817–830, 2003.

T. Chappex, L. Sofia-Gabrion, C. Dunant, and K. Scrivener. The effect of relative humidity and temperature on alkali expansion of mortar bars. In *Proc., 15th Int. Conf. on Alkali Aggregate Reaction in Concrete*, 2016.

L. Charpin and A. Ehrlacher. A computational linear elastic fracture mechanics-based model for alkali–silica reaction. *Cement and Concrete Research*, 42(4):613–625, 2012.

L. Charpin and A. Ehrlacher. Microporomechanics study of anisotropy of asr under loading. *Cement and Concrete Research*, 63:143–157, 2014.

I. Comby-Peyrot, F. Bernard, P.-O. Bouchard, F. Bay, and E. Garcia-Diaz. Development and validation of a 3d computational tool to describe concrete behaviour at mesoscale. application to the alkali-silica reaction. *Computational Materials Science*, 46(4):1163–1177, 2009.

C. Comi and U. Perego. Anisotropic damage model for concrete affected by alkali-aggregate reaction. *International Journal of Damage Mechanics*, page 1056789510386857, 2010.

C. Comi, B. Kirchmayr, and R. Pignatelli. Two-phase damage modeling of concrete affected by alkali–silica reaction under variable temperature and humidity conditions. *International Journal of Solids and Structures*, 49(23):3367–3380, 2012.

J. Dolbow, Z. Zhang, B. Spencer, and W. Jiang. Fracture capabilities in grizzly with the extended finite element method (x-fem). Technical report, Idaho National Laboratory (INL), Idaho Falls, ID (United States), 2015.

C. Dunant and K. Scrivener. Micro-mechanical modelling of alkali–silica-reaction-induced degradation using the amie framework. *Cement and Concrete research*, 40(4):517–525, 2010.

C. Dunant and K. Scrivener. Effects of uniaxial stress on alkali–silica reaction induced expansion of concrete. *Cement and concrete research*, 42(3):567–576, 2012a.

C. Dunant and K. Scrivener. Effects of aggregate size on alkali–silica-reaction induced expansion. *Cement and concrete research*, 42(6):745–751, 2012b.

M. Galassi, J. Davies, J. Theiler, B. Gough, G. Jungman, M. Booth, and F. Rossi. *GNU Scientific Library Reference Manual*. Network Theory Ltd. URL http://www.gnu.org/software/gsl, 2009.

D. Gaston, C. Newman, G. Hansen, and D. Lebrun-Grandie. Moose: A parallel computational framework for coupled systems of nonlinear equations. *Nuclear Engineering and Design*, 239(10):1768–1778, 2009.

G. Giaccio, R. Zerbino, J. Ponce, and O. Batic. Mechanical behavior of concretes damaged by alkali-silica reaction. *Cement and Concrete Research*, 38(7):993–1004, 2008.

E. Giannini. *Evalutaion of Concrete Structures Affected by Alkali-Silica Reaction and Delayed Ettringite Formation*. PhD thesis, University of Texas at Austin, 2012.

E. Giannini. Large-scale concrete mockups to study asr effects: Mix design update and recommendations. Technical report, University of Alabama, 2016.

A. Giorla. *Modelling of alkali-silica reaction under multi-axial load*. PhD thesis, École Polytechnique Fédérale de Lausanne, 2013.

A. Giorla, K. Scrivener, and C. Dunant. Influence of visco-elasticity on the stress development induced by alkali–silica reaction. *Cement and Concrete Research*, 70:1–8, 2015.

E. Grimal, A. Sellier, S. Multon, Y. Le Pape, and E. Bourdarot. Concrete modelling for expertise of structures affected by alkali aggregate reaction. *Cement and Concrete Research*, 40(4):502–507, 2010.

J. Hales, S. Novascone, R. Williamson, D. Gaston, and M. Tonks. Solving nonlinear solid mechanics problems with the jacobian-free newton krylov method. *Computer Modeling in Engineering & Sciences(CMES)*, 84(2):123–153, 2012.

N. Hayes, Q. Gui, S. Le Pape, L. Xiao, E. Giannini, R. Lenarduzzi, Y. Le Pape, and Z. Ma. Identification of mechanisms to study alkali-silica reaction effects on stress-confined concrete nuclear thick structures. In *3rd Conference on Technical Innovation in Nuclear Civil Engineering*, 2016.

H. Huang and B. Spencer. Grizzly model of fully coupled heat transfer, moisture diffusion, alkali-silica reaction and fracturing processes in concrete. In *9th International Conference on Fracture Mechanics of Concrete and Concrete Structures*, 2016.

H. Huang, B. Spencer, and G. Cai. Grizzly model of multi-reactive species diffusion, moisture/heat transfer and alkali-silica reaction for simulating concrete aging and degradation. Technical report, Idaho National Laboratory (INL), Idaho Falls, ID (United States), 2015.

T. Ichikawa and M. Miura. Modified model of alkali-silica reaction. *Cement and Concrete research*, 37(9): 1291–1297, 2007.

K. Kim, S. Jeon, J. Kim, and S. Yang. An experimental study on thermal conductivity of concrete. *Cement and Concrete Research*, 33(3):363–371, 2003.

V. Kodur, T. Wang, and F. Cheng. Predicting the fire resistance behaviour of high strength concrete columns. *Cement and Concrete Composites*, 26(2):141–153, 2004.

C. Larive. *Apports combinés de l'expérimentation et de la modélisation à la compréhension de l'alcali-réaction et de ses effets mécaniques*. PhD thesis, Ecole nationale des ponts et chaussees, 1997.

Y. Le Pape, Z. Ma, J. Cabage, and R. Lenarduzzi. Design of a large-scale concrete mockup to study the effects of alkali-silica reaction on expansion, damage and shear fracture propagation in stress-confined safety related structures. Technical Report M3LW-14OR-0403012 - Rev. 1, Light Water Reactor Sustainability Program, 2014.

A. Leemann and P. Lura. E-modulus of the alkali–silica-reaction product determined by micro-indentation. *Construction and Building Materials*, 44:221–227, 2013.

P. Léger, P. Côté, and R. Tinawi. Finite element analysis of concrete swelling due to alkali-aggregate reactions in dams. *Computers & structures*, 60(4):601–611, 1996.

Z. Ma, S. Le Pape, N. Hayes, Q. Gui, Y. Le Pape, R. Lenarduzzi, D. Clayton, and P. Ziehl. Alkali-silica-reaction test assembly - report describing the final instrumentation plan of the asr test assembly. Technical Report M3LW-16OR-040362, Light Water Reactor Sustainability Program, 2015.

J. Mazars. A description of micro-and macroscale damage of concrete structures. *Engineering Fracture Mechanics*, 25(5-6):729–737, 1986.

ML121160422. Impact of alkali silica reaction on seabrook concrete structure. Technical Report ML121160422, NextEra, 2012.

S. Multon. *Evaluation expérimentale et théorique des effets mécaniques de l'alcali-réaction sur des structures modèles*. PhD thesis, Université de Marne-la-Vallée, 2003.

S. Multon and A. Sellier. Multi-scale analysis of alkali–silica reaction (asr): Impact of alkali leaching on scale effects affecting expansion tests. *Cement and Concrete Research*, 81:122–133, 2016.

S. Multon and F. Toutlemonde. Effect of applied stresses on alkali–silica reaction-induced expansions. *Cement and Concrete Research*, 36(5):912–920, 2006.

S. Multon, M. Cyr, A. Sellier, P. Diederich, and L. Petit. Effects of aggregate size and alkali content on asr expansion. *Cement and Concrete Research*, 40(4):508–516, 2010.

H. Olafsson. The effect of relative humidity and temperature on alkali expansion of mortar bars. In *Proc., 7th Int. Conf. on Alkali Aggregate Reaction in Concrete*, pages 461–465, 1986.

J. Pan, Y. Feng, J. Wang, Q. Sun, C. Zhang, and D. Owen. Modeling of alkali-silica reaction in concrete: a review. *Frontiers of Structural and Civil Engineering*, 6(1):1–18, 2012.

R. Pignatelli, C. Comi, and P. Monteiro. A coupled mechanical and chemical damage model for concrete affected by alkali–silica reaction. *Cement and Concrete Research*, 53:196–210, 2013.

S. Poyet. Experimental investigation of the effect of temperature on the first desorption isotherm of concrete. *Cement and Concrete Research*, 39(11):1052–1059, 2009.

S. Poyet, A. Sellier, B. Capra, G. Thèvenin-Foray, J.-M. Torrenti, H. Tournier-Cognon, and E. Bourdarot. Influence of water on alkali-silica reaction: experimental study and numerical simulations. *Journal of Materials in civil Engineering*, 18(4):588–596, 2006.

C. Rabiti, A. Alfonsi, J. Cogliati, D. Mandelli, and R. Kinoshita. Reactor analysis and virtual control environment (raven) fy12 report. Technical report, Idaho National Laboratory report: INL/EXT-12-27351, 2012.

F. Rajabipour, E. Giannini, C. Dunant, J. Ideker, and M. Thomas. Alkali–silica reaction: current understanding of the reaction mechanisms and the knowledge gaps. *Cement and Concrete Research*, 76: 130–146, 2015.

G. Ranc, J. Sercombe, and S. Rodrigues. Comportement à haute température du béton de structure: impact de la fissuration sur les transferts hydriques. *Revue française de génie civil*, 7(4):397–424, 2003.

R. Reich, J. Cervenka, and V. Saouma. Merlin, a three-dimensional finite element program based on a mixed-iterative solution strategy for problems in elasticity, plasticity, and linear and nonlinear fracture mechanics. *EPRI Report, Palo Alto. Chapitre*, 1997.

H. Reinhardt and O. Mielich. A fracture mechanics approach to the crack formation in alkali-sensitive grains. *Cement and Concrete Research*, 41(3):255–262, 2011.

V. Saouma and M. Hariri-Ardebili. A proposed aging management program for alkali silica reactions in a nuclear power plant. *Nuclear Engineering and Design*, 277:248–264, 2014.

V. Saouma and L. Perotti. Constitutive model for alkali-aggregate reactions. *ACI materials journal*, 103(3): 194, 2006.

V. Saouma, L. Perotti, and T. Shimpo. Stress analysis of concrete structures subjected to alkali-aggregate reactions. *ACI structural journal*, 104(5):532, 2007.

L. A. Schoof and V. Yarberry. *EXODUS II: a finite element data model*. SAND92-2137, Sandia National Laboratories, Albuquerque, NM, 1994.

A. Shayan. Effects of naoh and nacl solutions and temperature on the behavior of specimens subjected to accelerated aar tests. *Cement and concrete research*, 28(1):25–31, 1998.

H. Shimizu, Y. Watanabe, H. Sekimoto, R. Oshima, K. Takiguchi, Y. Masuda, and I. Nishiguchi. Study on material properties in order to apply for structural analysis of turbine generator foundation affected by alkali-silica reaction. In *18th International Conference on Structural Mechanics in Reactor Technology (SMIRT 18)*, pages 2055–2060, Beijing, China, 2005. SMIRT18-H03-5.

T. Stanton. Expansion of concrete through reaction between cement and aggregate. *Proceedings of ASCE*, 66: 1781–1811, 1940.

A. Steffens, K. Li, and O. Coussy. Aging approach to water effect on alkali-silica reaction degradation of structures. *Journal of engineering mechanics*, 129(1):50–59, 2003.

R. Swamy and M. Al-Asali. Engineering properties of concrete affected by alkali-silica reaction. *ACI Materials Journal*, 85(5):367–374, 1988.

T. Takatura, T. Ishikawa, N. Matsumoto, S. Mitsuki, K. Takiguchi, and Y. Masuda. Investigation of the expanded value of turbine generator foundation affected by alkali-silica reaction. In *18th International Conference on Structural Mechanics in Reactor Technology (SMIRT 18)*, pages 2061–2068, Beijing, China, 2005. SMIRT18-H03-7.

J. Tcherner and T. Aziz. Effects of aar on seismic assessment of nuclear power plants for life extensions. In *Proceedings of the 20th International Conference on Structural Mechanics in Reactor Technology (SMIRT 20)*, number SMIRT20-Division 7 Paper 1789., Espoo, Finland, 2009.

A. Vayghan, F. Rajabipour, and J. Rosenberger. Composition–rheology relationships in alkali–silica reaction gels and the impact on the gel's deleterious behavior. *Cement and Concrete Research*, 83:45–56, 2016.

Y. Xi, Z. Bažant, L. Molina, and H. Jennings. Moisture diffusion in cementitious materials moisture capacity and diffusivity. *Advanced Cement Based Materials*, 1(6):258–266, 1994.

O. Zienkiewicz, M. Watson, and I. King. A numerical method of visco-elastic stress analysis. *International Journal of Mechanical Sciences*, 10(10):807–827, 1968.